A novel three-step mesa etching process for semiconductor lasers and the use of Monte Carlo simulations for active-width control

U. K. Chakrabarti and G. P. Agrawal
AT&T Bell Laboratories, Murray Hill, New Jersey 07974

(Received 21 September 1988; accepted for publication 13 February 1989)

This paper describes a new three-step mesa etching process for semiconductor lasers that allows fabrication of narrow active widths through the use of selective etching of individual layers of a double-heterostructure base material. The active width can be described by a simple analytic relation involving base material, etching, and lithographic parameters. Using this analytic relation, Monte Carlo simulations were used to obtain the distribution of the active width. Such simulations predict that the three-step etching process is expected to have a relatively high yield. The experimental distribution of the active width is in good agreement with the theoretical prediction.

INTRODUCTION

The fabrication of high-performance semiconductor lasers requires a buried heterostructure (BH) cavity[1,2] in which the active-region width is 1–2 μm and is controlled to within a small fraction of this value. The control of the active width is necessary since many laser characteristics depend critically on it. More specifically, the condition for operating in a single lateral mode as well as the modulation response depend on the active width.[3] A commonly accepted criterion for the active width is that it should be kept under 2 μm.[3,4] Two of the most important elements in BH laser fabrication are (1) the formation of a narrow (1–2 μm) mesa with defect-free side walls and (2) the confinement of the injected current to the active layer by epitaxially grown mesa-embedding layers. Recently BH lasers with low threshold current ($\lesssim$20 mA), high slope efficiency ($\sim$0.2 mW/mA/facet), and small-signal bandwidth (up to 14 GHz at 20 mW) have been reported by using devices where the mesa-embedding layer consists of iron-doped semi-insulating material (Fe:InP) and is grown either by vapor-phase epitaxy (VPE)[5] or by organometallic vapor-phase epitaxy (OMVPE).[6–9]

When OMVPE is used as a regrowth technology, several etching parameters, namely, the depth of mesa, the mask undercut and, more importantly, the shape of the mesa, need to be controlled carefully for obtaining a planarized growth of the mesa-embedding layer.[8,9] However, the VPE regrowth technology does not suffer from these restrictive requirements and can be used to planarize a reentrant mesa shape.[5,10]

The reentrant mesa shape is popular because it provides a narrow waist and a wide p^+-contact layer. Lasers with this type of mesa shape have been produced with low series resistance and stable fundamental mode operation.[4,10,11] Reverse mesa shape has been obtained by using a bromine–methanol mixture (Br/MeOH) of various proportions.[4,10–13] In this etching process depth variations of the active layer beneath the top surface translate into width variations. To overcome this difficulty, a two-step etching process has been demonstrated.[13]

In this paper we describe a novel three-step etching process that allows fabrication of lasers with narrow active widths through the use of selective etching of individual layers of a double-heterostructure base material. Furthermore, this etching procedure provides a wide p^+-contact layer. We also describe, using Monte Carlo simulations, a method to predict the distribution of the active width. The experimental results are in agreement with the theoretical predictions.

EXPERIMENT

Figure 1 shows the schematic of the etching process and is implemented in the following way. First, a grating with a periodicity of $\sim$2000 Å is fabricated on a (100)-oriented n-InP substrate using optical holography. Four epitaxial layers are then grown on the substrate using the liquid-phase epitaxial (LPE) growth technique. The layers are n-InGaAsP waveguide layer ($\lambda \sim 1.1$ μm), an undoped active layer ($\lambda = 1.3$ μm), a p-InP cladding layer, and a p-InGaAsP cap layer ($\lambda \sim 1.3$ μm). The last layer serves as the ohmic contact layer. To form the mesa etching mask, 3000 Å of SiO_2 is deposited and defined into stripes by standard photolithography [Fig. 1(a)]. The mesa etching procedure uses three sequential material-selective etchants. Using the SiO_2 mask, the contact quaternary layer (Q_c layer) is selectively etched in $10H_2SO_4$:$1H_2O_2$:$1H_2O$. This etchant etches InP at a negligible rate. During this etching step, the q layer is also etched under the mask producing an overhanging mask. The amount of mask undercut is defined by O_h [Fig. 1(b)]. Figure 2 shows the mask overhang O_h against etching time. During the initial stages of etching, O_h is almost linear with time, but after etching of the Q_c layer is over in the field region there is an increase in the undercutting rate. Next, the mesa is etched in solution C as prepared in the following way: Make a 80% HCl solution in H_2O and call it solution A; make solution B by mixing HBr and CH_3COOH in 1:1 ratio. Solution C is then prepared by mixing solutions A and B in 1:1 ratio. Solution C etches InP selectively and produces a reentrant profile [Fig. 1(c)]. The selective etching of InP by solution C is due to the fact that solutions A and B are themselves selective etchants of InP.[14] However, neither A nor B would provide a clean reentrant profile. To our knowledge, this is the first description of an etchant which selec-

Downloaded 26 Feb 2004 to 128.151.240.117. Redistribution subject to AIP license or copyright, see http://jap.aip.org/jap/copyright.jsp

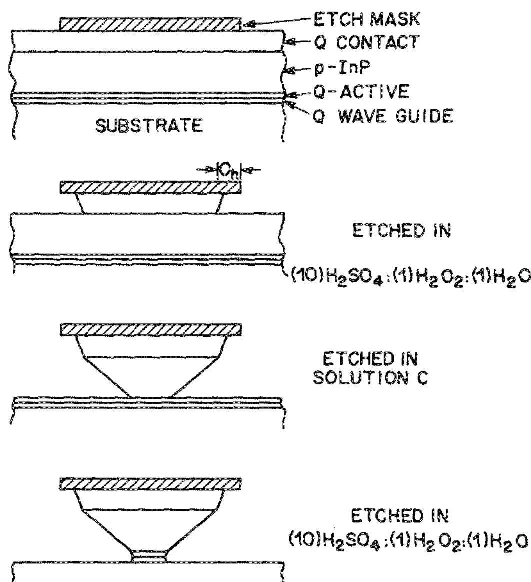

FIG. 1. Schematic illustration of the three-step etching process.

tively etches InP and also produces reentrant mesa profile. During the etching of InP, the quaternary layer acts as a mask. Similarly, using InP as a mask, the active layer is etched in $10H_2SO_4:1H_2O_2:1H_2O$ [Fig. 1(d)]. We did not observe any significant undercutting of the active layer. Figure 3 shows a scanning-electron-microscope picture of a cleaved cross section after completion of the etching. The inset shows the mesa with various geometrical parameters as defined in Table I.

Since the three-step etching process takes advantage of selective etching of different layers along specific crystal planes, the geometry of the mesa profile, and consequently the active width, can be accurately predicted. The active

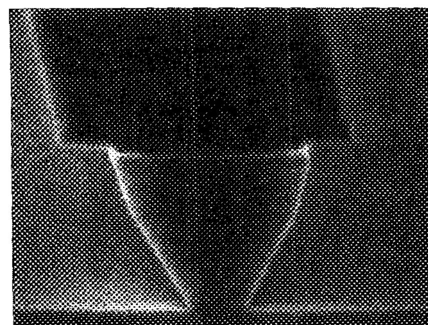

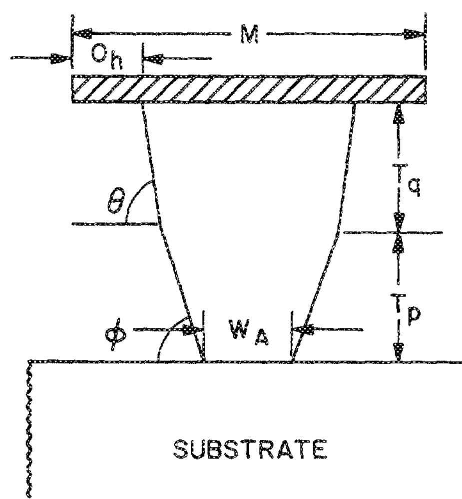

FIG. 3. (a) Scanning electron microscope picture of a cleaved cross section [{110} plane perpendicular to the (100) surface] showing the profile of an etched mesa. (b) Schematic cross section showing the various parameters used in the simulation. The range of values is given in Table I.

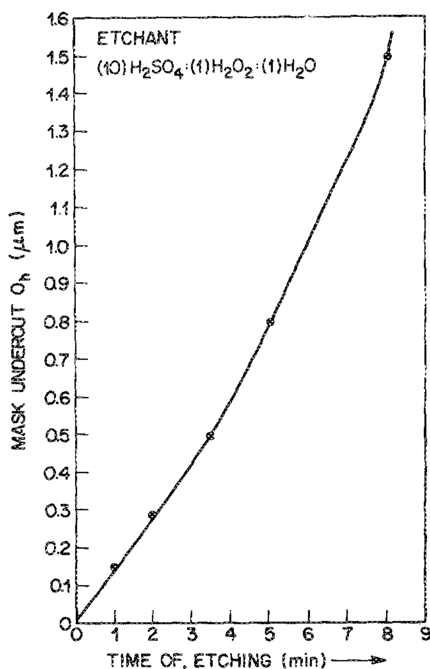

FIG. 2. Mask undercutting of the Q_c layer in $10H_2SO_4:1H_2O_2:1H_2O$.

width depends on several parameters such as the width M of the SiO_2 mask, the thickness T_q of the Q_c layer, and the thickness T_p of the p-type cladding layer. Since these parameters exhibit both intra- and interwafer variations, the resulting active width W_A varies from chip to chip over a certain range. We use the Monte Carlo technique to predict the distribution of the active width. This distribution can then be used to estimate the yield of the etch process for a specified range of W_A.

MONTE CARLO SIMULATION

The active width W_A from Fig. 3 is related to the device parameters M, T_p, and T_q by the relation

$$W_A = M - 2O_h - \alpha_p T_p - \alpha_q T_q, \quad (1)$$

where O_h is the overhang of the mask due to undercutting during selective etching of the quaternary contact layer. The etching constants α_p and α_q are related to angles ϕ and θ in Fig. 3 by the relations

$$\alpha_p = 2 \cot \phi, \quad \alpha_q = 2 \cot \theta. \quad (2)$$

These etching constants were determined experimentally from the scanning electron microscope pictures of cleaved

Downloaded 26 Feb 2004 to 128.151.240.117. Redistribution subject to AIP license or copyright, see http://jap.aip.org/jap/copyright.jsp

TABLE I. Range of parameter values used in Monte Carlo simulations.

Parameter	Symbol	Range
Mask width	M	5.5 ± 0.2 μm
q-contact layer thickness	T_q	$08. \pm 0.15\,\mu m$
p-cladding layer thickness	T_p	$1.5 \pm 0.15\,\mu m$
Mask overhang	O_h	1.0 ± 0.1 μm
Cladding-layer etching constant	α_p	1.07 ± 0.12
Contact-layer etching constant	α_q	0.53 ± 0.12

cross section of the etched mesa profiles (see Fig. 3 as an example). From measurements of more than 50 cross sections (from eight wafers) it was found that α_p and α_q have a mean and standard deviation given by

$$\overline{\alpha}_p = 1.07\ (\sigma = 0.06), \tag{3}$$

$$\overline{\alpha}_q = 0.53(\sigma = 0.06). \tag{4}$$

The mean values of α_p and α_q correspond to $\phi \simeq 62°$ and $\theta \simeq 75°$, respectively: ϕ is close to the angle associated with the plane {210} and θ is close to the angle associated with the plane {311}.

The value of O_h can be obtained from Eq. (1) for a targeted value of W_A and for given values of M, T_p, and T_q. In practice, the etching time is determined by O_h/R, where R is the etching rate which is estimated from Fig. 2. The three-step etching process has the advantage that the etching time can be optimized for individual wafers simply by estimating O_h from Eq. (1) for given values of M, T_p, and T_q. However, to account for both the intrawafer and interwafer variations in these parameters, we obtain the average value of the overhang using the average values of M, T_p, and T_q in Eq. (1), i.e.,

$$\overline{O}_h = \tfrac{1}{2}(\overline{M} - \overline{W}_A - \overline{\alpha}_p \overline{T}_p - \overline{\alpha}_q \overline{T}_q), \tag{5}$$

where $\overline{W}_A$ is the targeted active width, and $\overline{\alpha}_p = 1.07$ and $\overline{\alpha}_q = 0.53$ from Eqs. (3) and (4).

To demonstrate the predictability of the active-width distribution for the three-step etching process, we compare the prediction of the Monte Carlo simulations based on Eq. (1) with the experimental data. Figure 4 shows the experimental distribution of W_A for a sample of 74 laser chips from two wafers. Each wafer was etched for a target active width $W_A = 1.6\,\mu$m. The range of the parameters M, T_p, and T_q was also determined by measuring the mask width, the Q_c contact layer thickness, and the p-cladding layer thickness for these wafers. Table I lists the average values and the variation range of the six parameters that quantify the three-step etching process through Eq. (1). The probability distribution of these parameters is generally unknown. We have used the uniform distribution after assuming that all values are equally likely to occur. Although this need not be the case in practice, this choice corresponds to the worst case. The distribution of W_A is obtained simply by selecting M, O_h, α_p, α_q, T_p, and T_q randomly and calculating W_A from Eq. (1) for a sample size of 200. An increase in the sample size to 500 did not alter the results noticeably.

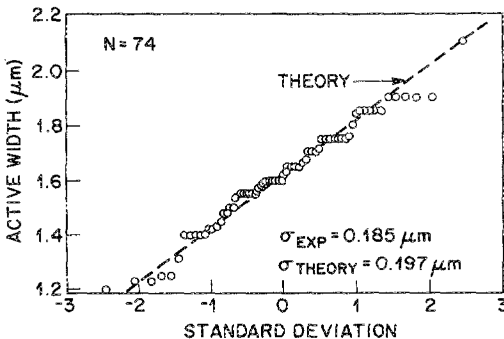

FIG. 4. Experimental distribution of the active width for 74 measurements over two wafers. The dashed line shows the theoretically calculated distribution by using Monte Carlo simulations.

The dashed line in Fig. 4 shows the calculated distribution of W_A using the Monte Carlo technique with the parameters of Table I. The target value of W_A was taken to be 1.6 μm. The distribution is approximately Gaussian, as evident by the linear nature of the normal probability plot. This is expected since W_A in Eq. (1) is a function of six independent random variables assumed to be identically distributed. We thus conclude that

$$p(W_A) = \frac{1}{\sigma\sqrt{2\pi}} \exp\left(- \frac{(W_A - \overline{W}_A)^2}{2\sigma^2} \right), \tag{6}$$

where $\overline{W}_A = 1.6\,\mu$m is the targeted value of W_A and σ is the standard deviation. For the distribution shown in Fig. 4, the calculated value is $\sigma \simeq 0.197\,\mu$m.

DISCUSSION AND CONCLUSION

A comparison of the experimental and calculated distributions in Fig. 4 reveals the main advantage of the three-step etching process. The experimental average active width of 1.62 μm is very close to the targeted value of 1.60 μm. The calculated value $\sigma = 0.197$ μm is slightly higher than the experimental value $\sigma = 0.185$ μm. This is due to our assumption of a uniform distribution for the parameters M, T_p, and T_q. Indeed, when a Gaussian distribution was used for these parameters, the calculated and experimental values of σ were found to be within 15%.

From the viewpoint of the success of a particular etching process, the figure of merit is the yield for a given tolerable range of W_A. We can estimate the yield of the three-step etching process by calculating the cumulative probability for $W_{min} \leqslant W_A \leqslant W_{max}$ or by using

$$Y(\sigma) = \int_{W_{min}}^{W_{max}} p(W_A)\, dW_A. \tag{7}$$

If we use Eq. (6) in (7), $Y(\sigma)$ can be expressed in terms of the error function as

$$Y(\sigma) = \frac{1}{2}\left[\mathrm{erf}\left(\frac{W_{max} - \overline{W}_A}{\sqrt{2}\sigma} \right) + \mathrm{erf}\left(\frac{W_A - W_{min}}{\sqrt{2}\sigma} \right) \right]. \tag{8}$$

As a simple application of Eq. (8), consider $W_{min} = 1.2\,\mu$m, $W_{max} = 2\,\mu$m, and $\overline{W}_A = 1.6\,\mu$m. Using the theoretical value $\sigma = 0.197\,\mu$m, we obtain $Y = 0.954$. Thus, the three-step etch process should provide 95% yield if the growth parameters are within the specifications of Table I.

Downloaded 26 Feb 2004 to 128.151.240.117. Redistribution subject to AIP license or copyright, see http://jap.aip.org/jap/copyright.jsp

We can estimate the yield degradation resulting from relaxing the parameter range by (i) calculating σ through the Monte Carlo technique and (ii) by using Eq. (8) with that calculated value of σ. As an example, if the range of T_p and T_q is enlarged from $\pm 0.15\,\mu$m to ± 0.2 mm, σ becomes $0.23\,\mu$m and using Eq. (8), we find that $Y = 0.918$. Thus, the yield is reduced from 95% to 92% because of the increased range of thickness variations for T_p and T_q. As a last example, we consider the increase in the range of O_h from $1.0 \pm 0.1\,\mu$m to $1.0 \pm 0.15\,\mu$m while at the same time keeping the enlarged ranges $T_p = 1.5 \pm 0.2\ \mu$m and $T_q = 0.8 \pm 0.2\ \mu$m. The calculated value $\sigma = 0.26\ \mu$m, and from Eq. (8) $Y = 0.877$. Thus, the yield further reduces to about 88% if the etching process results in a larger variation (0.85–1.15 μm) of the overhang. The important point to note is that the yield is not too sensitive to variations in the overhang.

To conclude, we have described a three-step etching process that is capable of providing excellent active-width control with relatively large yields. The existence of a simple analytic relation relating the active width to the etching parameters, the lithographic parameters, and the LPE growth parameters has enabled us to use Monte Carlo simulations to obtain the distribution of the active width resulting from intrawafer and interwafer variations in the above parameters. The active-width distribution is found to be nearly Gaussian. The calculated distribution is in good agreement with the experimental active-width distribution. Although this paper has focused on the application of the three-step etching process to a BH semiconductor lasers, the method is equally applicable to a Ridge waveguide design of semiconductor lasers.

[1]J. J. Hsieh and C. C. Shen, Appl. Phys. Lett. **30**, 429 (1977).

[2]H. Kano, K. Oe, S. Ando, and K. Sugiyama, Jpn. J. Appl. Phys. **17**, 1887 (1978).

[3]G. P. Agrawal and N. K. Dutta, *Long-Wavelength Semiconductor Lasers* (Van Nostrand Reinhold, New York, 1986).

[4]M. Hirao, A. Doi, S. Tsuji, M. Nakamura, and K. Aiki, J. Appl. Phys. **51**, 4539 (1980).

[5]S. Sugou, Y. Kato, H. Nishimoto, and K. Kasahara, Electron Lett. **22**, 1214 (1986).

[6]N. K. Dutta, J. L. Zilko, T. Cella, D. A. Ackerman, T. M. Shen, and S. G. Napholtz, Appl. Phys. Lett. **48** 1572 (1987).

[7]B. I. Miller, U. Koren, and R. J. Capik, Electron. Lett. **22**, 947 (1986).

[8]T. Sanda, K. Nakai, K. Wakao, M. Kuno, and S. Yamakoshi, Appl. Phys. Lett. **51**, 1054 (1987).

[9]U. K. Chakrabarti, Z. L. Zilko, T. Cella, N. Dutta, R. L. Brown, Y. Twu, J. W. Lee, and A. B. Piccirilli (unpublished).

[10]H. Temkin, R. A. Logan, R. F. Karlicek, K. E. Strege, and J. P. Blaha, Appl. Phys. Lett. **53**, 1156 (1988).

[11]R. A. Logan, H. Temkin, J. P. Blaha, and K. E. Strege, Appl. Phys. Lett. **51**, 1407 (1987).

[12]R. J. Nelson, R. B. Wilson, P. D. Wright, P. A. Barnes, and N. K. Dutta, IEEE J. Quantum Electron. **QE-17**, 202 (1981).

[13]S. Arai, M. Asada, T. Tanbun-ek, Y. Suematsu, Y. Itaya, and K. Kishino, IEEE J. Quantum Electron. **QE-17**, 640 (1981).

[14]S. Adachi, Y. Noguchi, and H. Kawaguchi, J. Electrochem. Soc. **129**, 1053 (1982).

Downloaded 26 Feb 2004 to 128.151.240.117. Redistribution subject to AIP license or copyright, see http://jap.aip.org/jap/copyright.jsp